THE JOURNAL OF PHYSICAL CHEMISTRY B

Article

pubs.acs.org/JPCB

PNP Diminishes Guanosine Glycosidic Bond Strength Through Restrictive Ring Pucker as a Precursor to Phosphorylation

Christopher B. Barnett and Kevin J. Naidoo*

Scientific Computing Research Unit and Department of Chemistry, University of Cape Town, Rondebosch 7701, South Africa

Supporting Information

ABSTRACT: Purine nucleoside phosphorylase is a transferase that catalyzes the addition of phosphate and removal of a purine base from guanosine and similar nucleosides. Here the interplay between sugar puckering conformation, the enzyme, and the perceived course of the reaction is examined using QM/MM FEARCF dynamics simulations. The enzyme biases the guanosine sugar ring toward a flattened ^4E conformer as a step that is critical to the success of the phosphorylation reaction. The C4′ endo conformer allows the nonbonded ring oxygen orbital to align and donate electrons into the antibonding glycosidic bond orbital, thus weakening the bond. This conformational preference is due to sustained and directed noncovalent interactions anchored by the phosphate nucleophile's hydrogen bonds to the sugar C2′ and C3′ hydroxyls. In so doing, PNP alters the solution sugar ring pucker preferences as part of its catalytic reaction barrier lowering function.

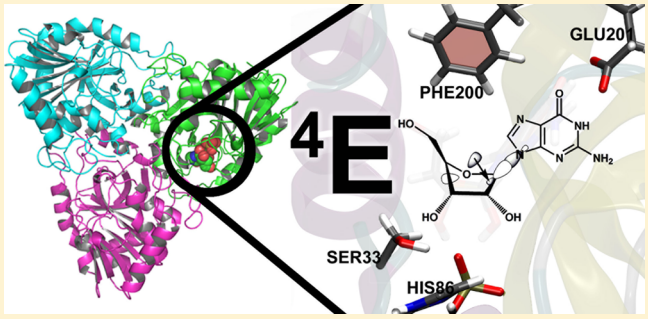

INTRODUCTION

The homotrimeric enzyme, purine nucleoside phosphorylase (PNP), catalyzes the reversible phosphorolysis of β-nucleosides to free purine base and ribose-α-1-phosphate and plays an important role in base salvaging pathways. Although the formation of the nucleoside is usually thermodynamically favored, the phosphorolysis direction is favored when the PNP reaction is coupled to purine base oxidation or phosphoribosylation (by xanthine oxidase or hypoxanthineguanine phosphoribosyltransferase respectively) due to rapid metabolic removal of purines.[1]

Deficiency of PNP[2] reduces the immune effect of T-cells causing developmental disorders and autoimmune disease. This is as a result of deoxy-guanosine-triphosphate (dGTP) build-up in tissues, especially in the lymph causing T-cell apoptosis.[3] Overactive T-cells can cause certain autoimmune disorders, tissue transplant rejection, and several cancers. Inhibition of PNP can be used to induce T-cell apoptosis, thus PNP has been targeted for rational drug design.[1a,3]

Bovine PNP (used in this study) is a homotrimer with P213 symmetry, and the active site is located at the interface between subunits; while mammalian PNPs share this symmetry, not all PNPs do so.[4] The exact nature of the PNP scaffold and the location of the binding sites for various substrates have been elucidated crystallographically. Similarly, in structure−function studies, where the steady-state kinetics of amino acid mutations[5] of PNP are analyzed, crystallographic techniques validate the mutation and are able to show modifications to the substrate binding mode.

Inhibitory drug studies originally focused on the use of substrate analogues of bovine PNPs. Inhibitors such as immucillin proved effective for bovine PNP at concentrations between 36 and 71 pM; however, the effectiveness is less pronounced for Human PNP.[6] A second generation of immucillin, DADMe immucillin with an extended linkage is more potent than the first-generation transition state (TS) analogues requiring as little as 6 pM for activity. The reaction proceeds via $D_N{\cdot}A_N$ and the extra linkage of the second generation immucillins is proposed to better mimic the dissociated TS of human PNP.[6] A third generation of inhibitors has been designed that contains an acyclic iminoalcohol to replace the cyclic mimic of the ribooxocarbenium ion at the transition states of PNPs. The best third-generation inhibitor is equivalent to the best inhibitors found in the previous generations TS analogues.[7]

The aim of PNP studies has centered around finding inhibitory drug targets in order to combat T-cell mediated autoimmune diseases.[1a,8] Key candidates for inhibitors of glycoenzymes are transition state analogues (TSAs) of the reactions catalyzed by the enzymes. Of critical importance to the design of these TSAs is the accurate representation of the carbohydrate (glycan) ring conformational pucker at the TS of the reaction in which the glycosidic bond forms or breaks.[9] The aim of this study is to evaluate the role of the PNP enzyme in prearranging the puckering conformation of the ribose sugar

Received: November 4, 2012
Revised: April 20, 2013
Published: April 26, 2013

dx.doi.org/10.1021/jp3109013 | J. Phys. Chem. B 2013, 117, 6019−6026

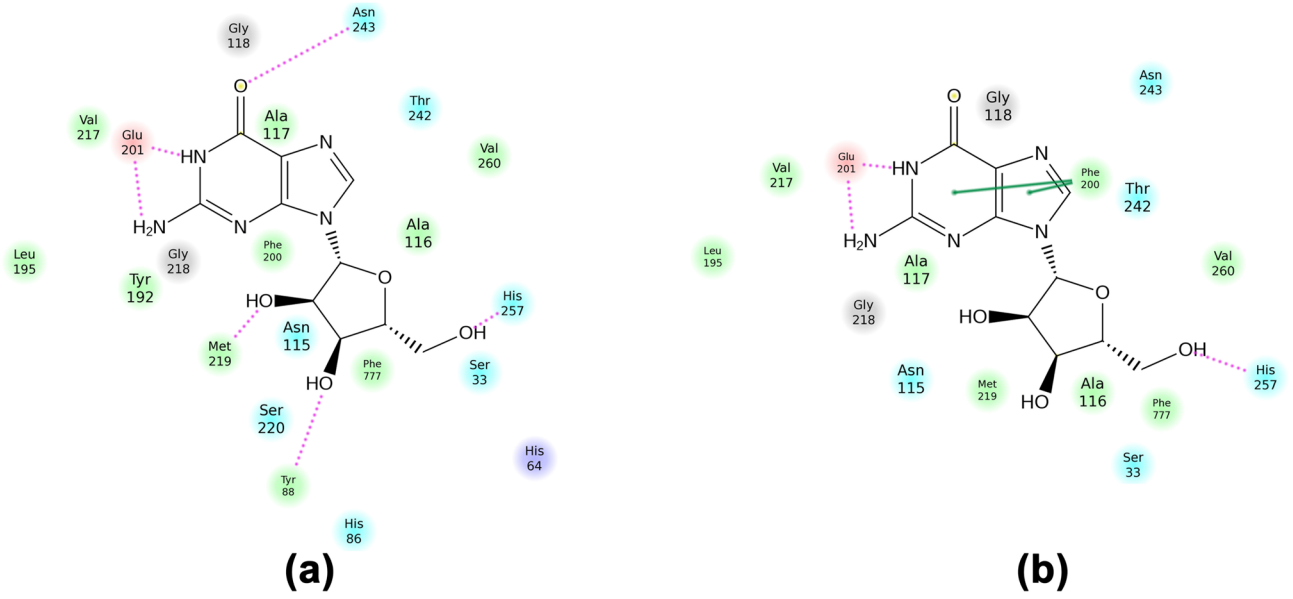

Figure 1. (a,b) Different poses of guanosine within PNP shown as 2D active site maps. Possible hydrogen bonding interactions are indicated with red stippled lines while hydrophobic interactions are indicated with green lines.

ring prior to the activation up to the TS. We employ a flat-histogram approach to calculate free energies of ring pucker. This is the free energies from adaptive reaction coordinate forces (FEARCF) method,[10] which includes an implementation of triangular tesselation puckering coordinates.[11]

A set of FEARCF calculations was carried out in vacuum and water, and the results were compared with the FEARCF enzyme results, the aim being to identify the role that the enzyme environment plays in preparing the guanosine nucleoside for phosphorylation. Considering the ribose vacuum pucker preferences,[12] the preference shown by guanosine in vacuum and in TIP3P water were identified. Following this, guanosine was placed in one of the symmetrically equivalent active sites of trimeric bovine PNP, and the enzyme induced pucker was determined by analyzing the puckering free energy surface (FES).

METHODS

PNP can catalyze phosphorylation in both the forward and reverse directions; however, the nucleoside was chosen over the phosphorylated sugar as most active site inhibitors of PNP are based on guanine derivatives. Guanosine was built in CHARMM using the CHARMM nucleic acid force field,[13] while the PNP was built using the CHARMM protein force field.[14] The guanosine and selected protein residues were then modeled quantum mechanically with SCC-DFTB/d[15] as described below in further detail (refer to Table S1 in the Supporting Information for a single point energy comparison between DFT and SCC-DFTB/d). Calculations were run with the mio-0-1 parameters,[16] and hydrogen bonding and dispersion effects were included with energies calculated based on

$$E[\rho_0(\vec{r})] = \sum_{i}^{occ} \langle \psi_i(\vec{r}) | h_i^{KS}[\rho_0(\vec{r})] | \psi_i(\vec{r}) \rangle + E_{rep} + \sum_{\alpha\beta} \Delta q_\alpha \Delta q_\beta \gamma_{\alpha\beta} - \sum_{\alpha\beta} f(R_{\alpha\beta}) \frac{C_6^{\alpha\beta}}{R^6} \quad (1)$$

Here we briefly detail the setup of the quantum mechanics/molecular mechanics (QM/MM) FES calculations for guanosine, water, and PNP that were carried out using CHARMM.[14] The FEARCF module can be interfaced with any molecular dynamics algorithm;[10b] however, in this study we coupled it to CHARMM. FEARCF is a flat histogram method. Using this approach to calculate the free energy of pucker the two-dimensional (2D) puckering coordinate space resulting from triangular tesselation, was discretized into a 2D grid. The sampling frequency for each bin site on the grid was recorded during each simulation. The potential of mean force (PMF)

$$W(\xi) = -k_B T \ln P(\xi) \quad (2)$$

where $W(\xi) = W(\theta_0,\theta_1)$ for the ring libration of ribose, was previously defined.[12] We use the same description here for guanosine in vacuum, water, and in bovine PNP (detailed later in Figure 3a). Briefly, the atomic forces that are applied to each of the ring atoms is recovered from the reaction coordinate forces by recasting them in terms of the PMF

$$\frac{\partial W(\xi)}{\partial \theta_i} = F(\theta_i) \quad (3)$$

The angle of puckering is calculated from

$$\theta_i = \pi/2 - \cos^{-1}[(q_i \cdot n)(\| q_i \| \cdot \| n \|)^{-1}] \quad (4)$$

and θ_0, $\theta_1 \in [-90°,90°]$.

The reference plane for the furanose ring was chosen as C3′-O4′-C2′ and the two ring flaps were defined as C3′-C4′-O4′ (θ_0) and O4′-C1′-C2′ (θ_1).

In vacuo VV2 dynamics of the guanosine was carried out at 298.15 K with group-based cutoffs of 10, 12, and 14 Å. The electrostatic and van der Waals potentials were treated with force shifting. The nonbonded interactions were updated using CHARMM's built-in heuristic algorithm. A FEARCF iteration comprised eight simultaneously run QM/MM simulations of guanosine in vacuum, each being 500 ps. At the conclusion of every FEARCF iteration, the histograms from each simulation were combined with those obtained in the previous iterations.

dx.doi.org/10.1021/jp3109013 | J. Phys. Chem. B 2013, 117, 6019−6026

This was carried out using our in-house multidimensional version of the weighted histogram method (WHAM[17]). The FEARCF generated surface was considered well-converged when the sampling ratio of highest to lowest energy regions on the FES, which were associated with canonical puckers, was at least 1:10. Convergence was reached within 20 iterations, achieving a ratio of 1:5.

The minimized coordinates from the vacuum calculations were solvated in a cube of side 33.98 Å with 1315 TIP3P[18] waters. The system was then heated for 30 ps and equilibrated for 100 ps with the same dynamics specification as for vacuum. The equilibrated system was employed to start the free energy calculations. Water VV2 dynamics of the guanosine was carried out at 298.15K with atom-based cutoffs of 10, 12, and 14 Å. The electrostatic and van der Waals potentials were treated with force shifting. The nonbonded interactions were updated using CHARMM's built-in heuristic algorithm. Shake was applied to all MM atoms. Periodic boundary conditions were applied, and the cutoff was chosen at 14 Å. A FEARCF iteration comprised eight simultaneously run QM/MM simulations of guanosine in water each being 500 ps. Convergence was reached in sixteen iterations achieving a ratio of 1:5.6.

The 1A9S bovine PNP structure as reported by Ealick[19] was protonated following a pK_a analysis. Several amino acids are conserved across PNP from different organisms.[8] The trimeric form was built using the SYMMETRY records in the PDB, and the atoms were placed using VMD.[20] One active site of the three available was chosen to conduct the experiment. The waters of crystallization were not removed.[5a] Depending on the dynamic structure of the binding pocket and movement of the substrate, different poses (positions and conformations) of the substrate may be identified.[21] Figure 1 demonstrates possible hydrogen-bonding motifs for Glu201, Asn243, Met219, and Tyr88 and π-stacking interactions for Phe200.

HPO_4^{2-} is modeled in the binding pocket using the CHARMM force field. This is done deliberately, as we are not aiming to explore the phosphorylation reaction FES. Guanosine, Ser33, Phe200, Glu201, and His257 make up the quantum region of the active site in Figure 2 and general hybrid orbitals (GHOs)[22] join the QM and MM regions. The amino acids are selected based on mutation studies, their conservation across species, and on the ability to interact with both the sugar and base moieties of guanosine. After initial minimization, a 24.5 Å TIP3P water sphere was positioned over guanosine in the active site of PNP. After heating and equilibration, FEARCF pucker simulations were conducted. For each iteration of the FEARCF, eight 200 ps QM/MM protein FEARCF calculations were run until convergence (nine iterations). Langevin Verlet dynamics with stochastic boundaries were employed for the protein QM/MM simulations. The final sampling ratio (most probable pucker:least probable pucker) for a single FEARCF run was 1:17.8 (ninth iteration).

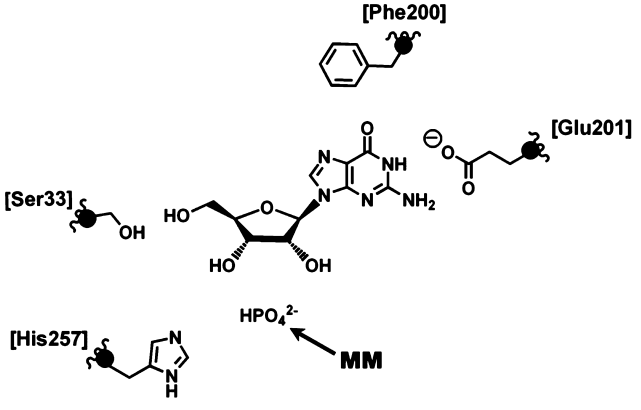

Figure 2. The PNP active site showing the classically modeled HPO_4^{2-} ion as well as quantum residues. GHO atoms are represented as black spheres.

Electronic Structure Analysis and DFT Calculations. Selected guanosine pucker conformers were extracted from CHARMM using the MMQM module. QM energy calculations were carried out with and without external molecular charges in Gaussian 03[23] using RB3LYP/6-31+G**. A natural bond orbital (NBO) analysis was performed with the Gaussian NBO version 3.1 by applying the RESONANCE keyword.[24] Atoms-in-molecules (AIM) calculations[25] were carried out on optimized guanosine structures from vacuum and PNP simulations and from the PDB (1A9S and 1RFG). These structures were optimized in Gaussian 03 using the RB3LYP/6-311+G** basis set.

RESULTS AND DISCUSSION

Furanosyl Ring Flexibility. Guanosine, a furanose derivative, is analyzed similarly to ribose.[12] The furanose ring is triangularly tesselated into three planes (Figure 3a). The central plane is used as a reference from which the angles (θ_0 and θ_1) that the adjacent planes make with it are calculated. The familiar (10 envelope (E), 10 twist (T), and 1 planar) canonical conformers can be mapped onto a discretized grid of all possible θ_0 and θ_1 angles (Figure 3b). The perfect *canonical* conformers are derived from the homocyclic cyclopentane ring. The black lines originating from the center planar conformer

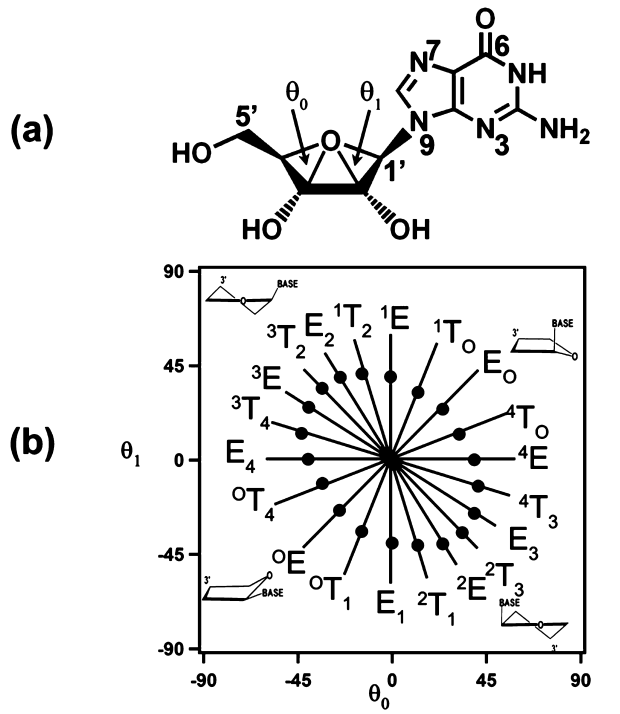

Figure 3. (a) Guanosine labeled with the puckering angles derived from the triangular tesselation scheme. (b) The pucker phase space resulting from a triangular tesselation of five-membered rings with C3′−O4′−C2′ as the reference plane.

dx.doi.org/10.1021/jp3109013 | J. Phys. Chem. B 2013, 117, 6019−6026

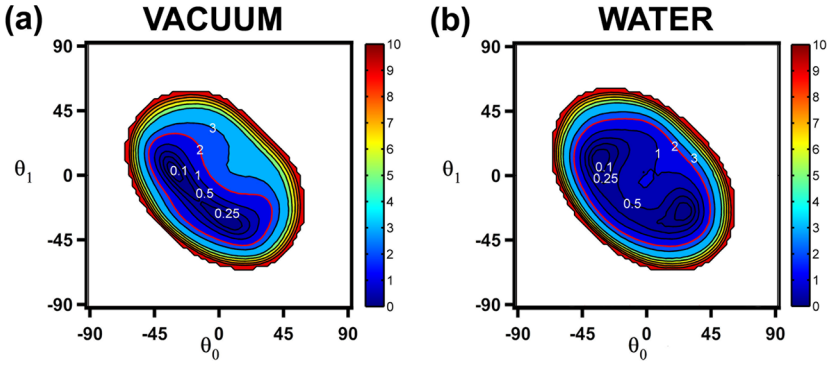

Figure 4. The converged FES of pucker for guanosine in (a) vacuum and (b) in water shown as two-dimensional contour plots where the area that is 2 kcal/mol about the global minimum is demarcated with a pink line. The energy is contoured from 0 kcal/mol (blue) to 10 kcal/mol (red).

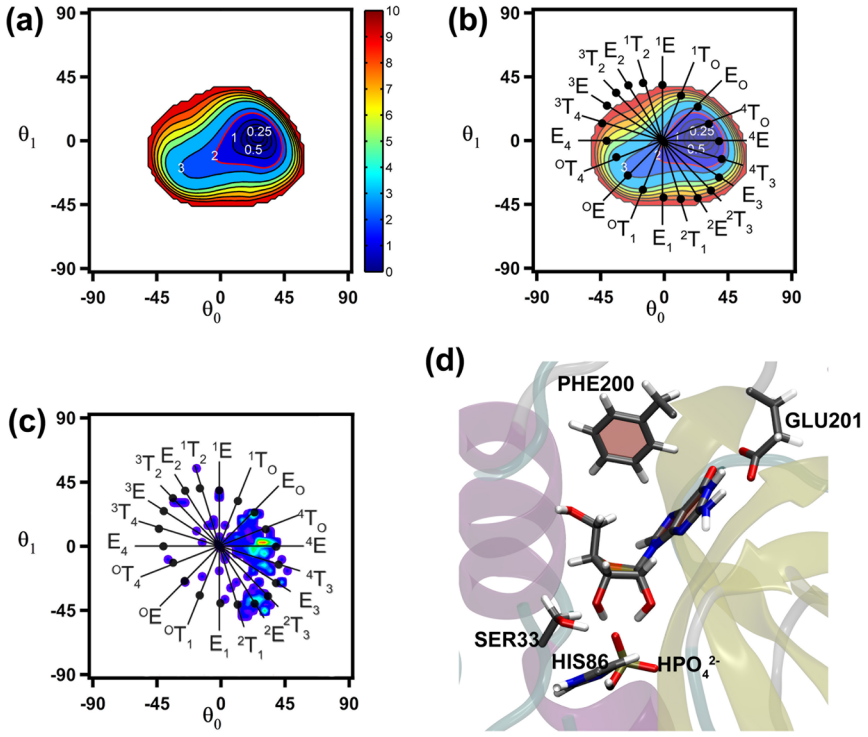

Figure 5. (a) The free energy map obtained for guanosine in the active site of PNP. The free energy is been mapped to color from 0 kcal/mol (blue) to 10 kcal/mol (red). The thermally accessible conformational space is demarcated by the pink contour line. (b) The pucker definitions overlaid on FES. (c) The pucker definitions overlaid onto a normalized probability distribution of ribofuranose puckering in PNP's taken from the PDB. Red represents high probability (includes the ^4E pucker). (d) The ^4E conformer of guanosine in the active site of PNP.

represent regions along which heterocyclic ring conformers may be found.

To better understand the environmental effect on the puckering of the ribofuranose ring, we directly compare the puckering FES in vacuum, TIP3P water, and in the PNP binding pocket. The vacuum pucker FES (Figure 4a) reveals a wide area that is within 2 kcal/mol of the global minimum[26] C4′ *exo* conformer (E_4). This area is demarcated with a pink contour line, indicating that conformers that are inside this region are not individually observable for long periods as their energy separations are below the reservoir of available thermal energy (3kT or 1.8 kcal/mol at 298.15K). In vacuum, the ring undergoes free interchange between several canonical conformations. The nearby C3′ *endo* ($^3T_4$) ring pucker conformer residing at (−32.5°, 5.0°) and the C2′ *endo* ($^2T_1$) conformer present at (13.75°,−17.5°) as well as the coexistence of $^3T_4$, $^2T_1$, and E_1 that are within 0.1 kcal/mol of the global minima makes interchange between these minima easily achievable at 298.15 K since a barrier of only 0.3 kcal/mol ($<kT$) separates them.

Despite the myriad of ring shapes available, the planar conformer, which is of central importance to the stability of an oxacarbenium ion, which is 2.6 kcal/mol higher in energy than the E_4 conformer, is not spontaneously expected to form in vacuum. Further, not all of the canonical conformers are within the thermal envelope; to achieve this requires 4 kcal/mol.

The guanosine vacuum puckering is notably different from ribose. It was shown previously[12] that ribose prefers C3′ *endo* and O4′ *exo* puckering, while here we see that guanosine prefers O4′ *endo* puckering. Further, the ring conformational space is more constrained for guanosine than for ribose.

In water, the guanosine pucker FES (Figure 4b) reveals an even less confined space than in vacuum. This can be seen from the larger thermally accessible pucker space (enveloped by the

dx.doi.org/10.1021/jp3109013 | J. Phys. Chem. B 2013, 117, 6019−6026

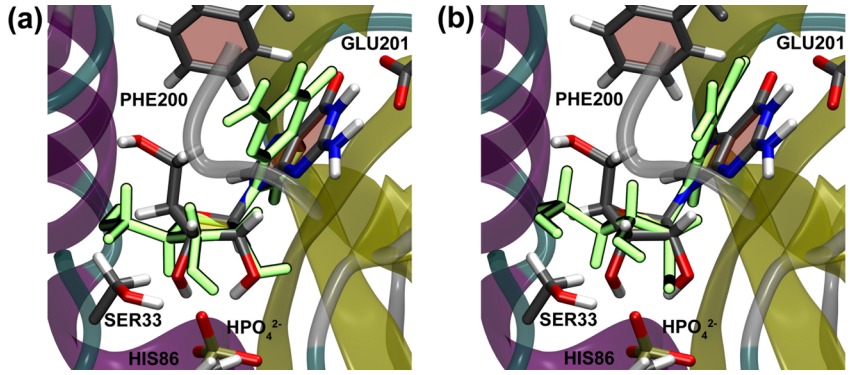

Figure 6. (a) The active site of PNP (shown in the background) binding the ^4E ribose conformer of guanosine as found in PNP free energy simulations as well as the E_4 conformer of guanosine as found in vacuum (highlighted) free energy simulations. (b) The active site of PNP (shown in the background) hosting the ^4E conformer of guanosine as found in PNP free energy simulations as well as $^3T_4$ conformer of guanosine from water studies highlighted.

pink 2 kcal/mol contour line). The structure has two favorite ring puckers in water. These are a $^3T_4$ conformer at (−32.5°, 10°) and a $^2T_3$ conformer at (26.5°, 25.0°). This is reminiscent of the North ($^3T_2$)↔South ($^2T_3$) two-state interchange observed in α nucleosides[27] via a $^3T_4 \rightarrow E_4 \rightarrow {}^OT_4 \rightarrow {}^OE \rightarrow {}^OT_1 \rightarrow E_1 \rightarrow {}^2T_1 \rightarrow {}^2E \rightarrow {}^2T_3$ minimum free energy path. The O4′ *endo* (^OE) is the transition state at (−20°,−17.5°) that separates the C3′ *endo* minima from the C2′ *endo* minima with a barrier of 0.4 kcal/mol. The planar conformer is energetically accessible being only 1.01 kcal/mol above the global energy minimum. Equally other flat ring structures in close proximity to it are equally accessible with a maximum of 1.0 kcal/mol at (0°, −2.5°) and a TS of 0.5 kcal/mol located at (5.0°, 0.0°). Therefore, compared with the vacuum case guanosine can pucker relatively easily into the planar conformer in water away from the preferred minimum energy ring structures. However, the increased conformational flexibility of guanosine in water lowers the probability of a planar ring conformation that stabilizes the oxocarbenium ion formation necessary for the occurrence of a transition state. This is because the planar structures are in competition with a wide variety of other ring puckers at room temperature. Nonetheless, an important similarity between the vacuum and water environments is that the ring conformers prefer O4′ *endo* structures as this orientates the bulky base away from the O4′ lone pairs. In water, the biasing is less pronounced, as the solvent interferes with the stereo electronic relationship between the ring oxygen and primary alcohol complex, as we have shown for the pyranosyl case.[28]

Furanosyl Ring Pucker Preferences in PNP. While the sugar ring in guanosine increases its conformational flexibility in water compared with vacuum, accessing all of conformational space, a diametrically opposite scenario unfolds when it is bound to the PNP in the catalytic site. The enzyme dramatically restricts the ribose ring pucker and the base flipping. Only O4′ *exo* (E_O,^4T_O), C3′ *exo* (E_3), C4′ *endo* (^4E,$^4T_3$) and C2′ *endo* ($^2T_3$,^2E) can be thermally accessed, where ^4E is the global minimum at (25°, 2.5°) on the puckering FES (Figure 5a). This is the only stationary point on the FES.

A geometrical analysis of the 21 conformers accessible to a five-membered ring show that only the planar, E_3 and ^3E conformers can form a full character oxocarbenium ion.[29] Interestingly, Kinetic Isotope Effect (KIE) studies coupled with QM optimization strongly indicated that ^{3}E and E$_3$ exist at the TS for the PNP reaction for inosine.[30] It is therefore surprising to discover that ^4E is the most favored conformer (Figure 5a,b) on the PNP pucker FES, as it cannot form an oxocarbenium ion, which is critical to TS formation.

However, there is overwhelming crystallographic evidence supporting the preference of guanosine ^4E puckering (Figure 5c) when it is bound to the PNP catalytic site. An analysis of several PDBs containing guanosine or similar molecules (adenosine, inosine, 3DG) 1JE1,[31] 1RFG,[32] 3IEX,[4] 1PK7,[33] 1A9S[19] (the one used in this study), 1PR0,[33] 1V45[32] (with 3DG) show ribose favoring an ^4E conformer. Other conformers can exist for nucleosides, for example inosine adopts E_4 in 1RCT[34] (human PNP), while crystal structures containing ribose-1-phosphate, 1A9T[19] and 3FB1,[21] do not exhibit ^4E conformers; 3FB1 has E_3 conformers and E_2 conformers. In contrast to the guanosine substrate, the conformers of TSAs inhibitors, such as immucillin-H, adopt a planar or almost planar conformer (e.g., 1RT9, 1RR6, Human PNP) (10.2210/pdb1rt9/pdb).[35] A statistical analysis of all the available PNP enzymes with five-cycle substrates shows that the ^4E pucker conformer is commonly found in the active site (Figure 5c and Supporting Information). Our QM/MM simulations indicate that the C2′ and C3′ hydroxyl groups strongly interact with the phosphate anion while it is in the vicinity of the guanosine, encouraging the formation of the ^4E conformer (Figure 5d).

Other C4′ *endo* (^4T_O and $^4T_3$) conformers are adjacent to ^4E and separated from it by approximately 0.5 kcal/mol. More than 10 kcal/mol is required to reach all canonical pucker conformers since the PNP catalytic site severely restricts the available puckering conformational space. This observation is supported by a comparison of the vacuum, water, and PNP pucker FES′ contoured at 3kT (Supporting Information, Figure S1). The PNP ribose pucker FES accessible at room temperature is smallest since guanosine cannot undergo large scale movements in the binding site as it is being constrained by the size of the binding site cavity and specific amino acid interactions with Ser33 and His257 that hold the anchoring phosphate (Figures 5 and 6) in place.

It appears that PNP preactivates the substrate by limiting the ring pucker conformational freedom to a pucker that favors oxocarbenium ion formation. This puckering limitation is induced by strong electrostatic interactions between the ribose sugar and the phosphate nucleophile. This conclusion is drawn from a normalized probability distribution calculated from eight combined 1 ns QM/MM trajectories. In that distribution, the phosphate oxygens, particularly O4, have a strongly preferred

dx.doi.org/10.1021/jp3109013 | J. Phys. Chem. B 2013, 117, 6019−6026

interaction with the hydrogens of the 2 and 3-hydroxyl group of guanosine. The phosphate distance was binned relative to the puckering conformer observed, and a predominance of ^4E-like conformers were observed (Supporting Information, Figure S2). Further evidence of the conformational limitation placed on the guanosine by PNP is found by overlaying multiple guanosine root-mean-square deviation (RMSD) fitted structures over the course of eight 1 ns QM/MM trajectories in vacuum, water, and protein (Figure 7). In vacuum and water,

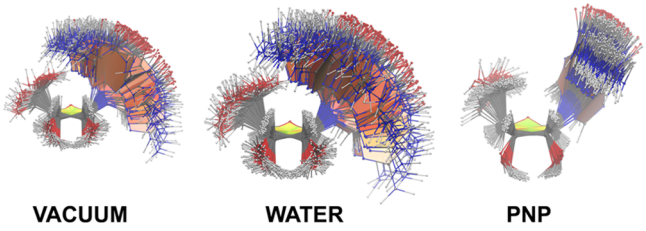

Figure 7. Four hundred overlaid frames of eight 1 ns trajectories of guanosine, water, and PNP. These frames were RMSDs aligned to the sugar ring (O4′ C1′ C2′ C3′ C4′).[20]

the movement of the purine moiety has motional freedom, while in PNP this is not the case. Although we do not explicitly indicate it here, it is plausible that the ring pucker conformation shows distinct preferences during the course of the reaction as shown previously for CBHI.[36] Nonetheless, from the free energy simulations and PDB analyses presented here, we see that PNP flattens the furanosyl ring into an ^4E ring pucker in preparation of the phosphorylation reaction.

The ^4E conformer is achieved principally from a strong electrostatic interaction between the phosphate ion and hydroxyls on the sugar ring (Figure 5d). An overlay of ^4E guanosine with in vacuo E_4 and water $^3T_4$ conformers aligned along the C−N bond and placed in the active site of PNP suggests important molecular differences between them (Figure 6). This is the result of the C2′ and C3′-hydroxyl group interactions with HPO_4^{2-} and the Glu201 hydrogen bonding to the base. The position of the base moiety of guanosine is due to the Glu201 hydrogen bonding motif and interaction with the Phe200. The sugar pucker conformer is determined mainly by the pulling effect of the phosphate nucleophile, which is not present in water (note the optimized hydrogen bonding made by the hydroxyl groups).

The role that HPO_4^{2-} plays in toggling the C2′ and C3′-hydroxyl groups using electrostatic binding to achieve ^4E ribose puckering is central to map the reaction path toward a TS. Here the HPO_4^{2-} was modeled using classical parameters and so the phosphorylation reaction cannot take place. However, we observed that the once the phosphate has steered the ribose ring to a flattened ribose pucker in PNP, a minor lengthening of the glycosidic bond is observed compared with the vacuum SCC-DFTB simulations. The global minimum guanosine structures found in vacuum and in a field of PNP enzyme charges were therefore subjected to DFT level optimizations (B3LYP/6-311+G**). The optimized global minimum vacuum structure has a glycosidic C1′−N9 bond length of 1.455 Å, while in the PNP environment the bond is lengthened to 1.480 Å. A survey of experimental crystal structures deposited in the PDB, particularly the guanosine ligand in the active site of Human PNP, revealed that the C−N bond is similar in length to our optimization calculation (Table 1). The related

Table 1. The Change in Bond Length and Electron Density in the *N*-Glycosidic Bond (C1′−N9) of Guanosine in Vacuum and PNP

environ	bond length (Å)	ρ
vacuum	1.455	0.261
PNP[a]	*1.480*	0.248
PNP[b]	*1.480*	0.245
PNP[c]	*1.550*	0.218

[a]Guanosine obtained from the reaction dynamics QM/MM simulation and optimized in the field of PNP charges. [b]Guanosine from PDB 1RFG (Human PNP). [c]Inosine from PDB 1A9S (Bovine PNP).

nucleoside inosine in bovine PNP has a longer bond length. A calculation of the electron density (ρ) in the C1′−N9 bond using the AIM method confirmed that the electron density trend inversely correlates with the bond length (Table 1) i.e., the vacuum structure has the shortest bond length and largest electron density. Therefore prior to the transition state, the C1′−N9 bond of guanosine in PNP is lengthened and weakened.

To better understand the relationship between the increase in glycosidic bond length and the ^4E pucker correlated ring pucker, we performed an NBO analysis of the minima and transition puckering conformers (Table S2, Figure 8) in vacuum, water, and PNP. From this analysis, we hypothesize that the ring oxygen nonbonding orbital ($n_{O4'}$) significantly contributes electrons to the antibonding $\sigma^*_{C1'-N9}$ orbital ($n_{O4'} \rightarrow \sigma^*_{C1'-N9}$) when guanosine is in the preferred C4′ endo

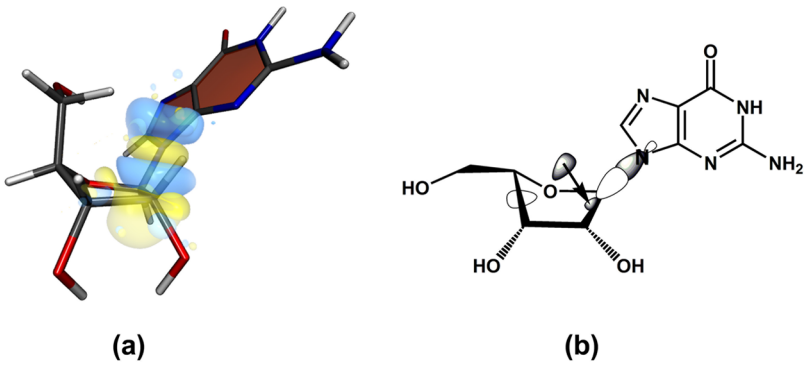

Figure 8. (a) A molecular representation of guanosine with the NBOs for the $n_{O4'} \rightarrow \sigma^*_{C1'-N9}$ transition overlaid. (b) Schematic of the electronic donation from the ring oxygen orbital to the antibonding orbital of the glycosidic bond.

dx.doi.org/10.1021/jp3109013 | J. Phys. Chem. B 2013, 117, 6019−6026

conformer (^4E pucker) in PNP. We propose that this may lead to the weakening of the glycosidic bond (C1′−N9) which will contribute to the lowering of the reaction barrier for nucleophilic attack by the HPO_4^{2-} nucleophile at C1′ leading to phosphorylation. The particular puckering conformer is a result of the two sugar hydroxyl groups that hydrogen bond to the phosphate nucleophile coupled with the restriction of base movement (i.e., brought about by Glu201 hydrogen bonding motif and interaction with the Phe200) in the catalytic pocket.

CONCLUSION

The PNP active site significantly limits sugar pucker space compared with vacuum and water cases. Moreover in PNP, the ring pucker in the guanosine substrate is biased toward the ^4E puckering conformer, which is diametrically opposed to the two preferred puckering minima observed in vacuum (E_4 and E_1) and the two preferred puckering minima observed in water ($^3T_4$ and $^2T_3$). This ^4E conformer observed in these free energy of pucker calculations echoes the pucker conformations of nucleosides observed in PNP's numerous crystal structures. However, the ^4E conformer is not the same as ^3E, E_3, or the planar conformations proposed for the PNP reaction TS. While this C4′ *endo* conformer cannot form an oxocarbenium ion, it appears to be a critical step on the path toward the TS. This is because this ^4E conformer comes about through the strong hydrogen bonding interactions that the incoming phosphate nucleophile forms with the hydroxyls at C2′ and C3′. In so doing, the nonbonding orbital on the ring oxygen is then aligned with the antibonding C1′−N9 orbital resulting in electron donation, $n_{O4'} \rightarrow \sigma^*_{C1'\text{-}N9}$, and a weakening of the glycosidic bond.

ASSOCIATED CONTENT

Supporting Information

Additional figures, coordinates, and PDB data are deposited. This material is available free of charge via the Internet at http://pubs.acs.org.

AUTHOR INFORMATION

Corresponding Author

*E-mail: Kevin.Naidoo@uct.ac.za. Tel: +27-21-650-2542. Fax: +27-21-686-4333.

Author Contributions

The manuscript was written through contributions of all authors. All authors have given approval to the final version of the manuscript.

Notes

The authors declare no competing financial interest.

ACKNOWLEDGMENTS

This work is based upon research supported by the South African Research Chairs Initiative (SARChI) of the Department of Science and Technology and National Research Foundation to K.J.N. C.B. thanks the SARChI for doctoral fellowship support.

ABBREVIATIONS

FEARCF free energies from adaptive reaction coordinate force; PNP purine nucleoside phosphorylase; QM/MM quantum mechanics/molecular mechanics; TSAs transition state analogues

REFERENCES

(1) (a) Erion, M. D.; Takabayashi, K.; Smith, H. B.; Kessi, J.; Wagner, J.; Hönger, S.; Shames, S. L.; Ealick, S. E. Purine Nucleoside Phosphorylase. 1. Structure-Function Studies. *Biochemistry* **1997**, *36*, 11725−11734. (b) Deng, H.; Cahill, S. M.; Abad, J.-L.; Lewandowicz, A.; Callender, R. H.; Schramm, V. L.; Jones, R. A. Active Site Contacts in the Purine Nucleoside Phosphorylase Hypoxanthine Complex by NMR and *ab initio* Calculations. *Biochemistry* **2004**, *43*, 15966−15974.

(2) Markert, M. L. Purine Nucleoside Phosphorylase Deficiency. *Immunodefic. Rev.* **1991**, *3*, 45−81.

(3) Kicska, G. A.; Schramm, V. L.; Long, L.; Fairchild, C.; Tyler, P. C.; Furneaux, R. H.; Hörig, H.; Kaufman, H. L. Immucillin H, a Powerful Transition-State Analog Inhibitor of Purine Nucleoside Phosphorylase, Selectively Inhibits Human T Lymphocytes. *Proc. Natl. Acad. Sci. U.S.A.* **2001**, *98*, 4593−4598.

(4) Castilho, M. S.; Postigo, M. P.; Pereira, H. M.; Oliva, G.; Andricopulo, A. D. Structural Basis for Selective Inhibition of Purine Nucleoside Phosphorylase from *Schistosoma mansoni*: Kinetic and Structural Studies. *Bioorgan. Med. Chem.* **2010**, *18*, 1421−1427.

(5) (a) Saen-oona, S.; Quaytman-Machledera, S.; Schramm, V. L.; Schwartz, S. D. Atomic Detail of Chemical Transformation at the Transition State of an Enzymatic Reaction. *Proc. Natl. Acad. Sci. U.S.A.* **2008**, *105*, 16543−16548. (b) Ealick, S. E.; Babu, Y. S.; Bugg, C. E.; Erion, M. D.; Guida, W. C.; Montgomery, J. A.; Secrist, J. A. Application of Crystallographic and Modeling Methods in the Design of Purine Nucleoside Phosphorylase Inhibitors. *Proc. Natl. Acad. Sci. U.S.A.* **1991**, *88*, 11540−11544.

(6) Lewandowicz, A.; Tyler, P. C.; Evans, G. B.; Furneaux, R. H.; Schramm, V. L. Achieving the Ultimate Physiological Goal in Transition State Analogue Inhibitors for Purine Nucleoside Phosphorylase. *J. Biol. Chem.* **2003**, *278*, 31465−31468.

(7) Taylor, E. A.; Clinch, K.; Kelly, P. M.; Li, L.; Evans, G. B.; Tyler, P. C.; Schramm, V. L. Acyclic Ribooxacarbenium Ion Mimics as Transition State Analogues of Human and Malarial Purine Nucleoside Phosphorylases. *J. Am. Chem. Soc.* **2007**, *129*, 6984−6985.

(8) Erion, M. D.; Stoeckler, J. D.; Guida, W. C.; Walter, R. L.; Ealick, S. E. Purine Nucleoside Phosphorylase. 2. Catalytic Mechanism. *Biochemistry* **1997**, *36*, 11735−11748.

(9) (a) Zechel, D. L.; Withers, S. G. Glycosidase Mechanisms: Anatomy of a Finely Tuned Catalyst. *Acc. Chem. Res.* **2000**, *33*, 11−18. (b) Lairson, L. L.; Henrissat, B.; Davies, G. J.; Withers, S. G. Glycosyltransferases: Structures, Functions, and Mechanisms. *Annu. Rev. Biochem.* **2008**, *77*, 521−555.

(10) (a) Strümpfer, J.; Naidoo, K. J. Computing Free Energy Hypersurfaces for Anisotropic Intermolecular Associations. *J. Comput. Chem.* **2010**, *31*, 308−316. (b) Naidoo, K. J. FEARCF, a Multidimensional Free Energy Method for Investigating Conformational Landscapes and Chemical Reaction Mechanisms. *Sci. China, Ser. B: Chem.* **2011**, *54*, 1962−1973. (c) Naidoo, K. J. Multidimensional Free Energy Volumes Offer Unique Insights into Reaction Mechanisms, Molecular Conformation, and association. *Phys. Chem. Chem. Phys.* **2012**, *14*, 9026−9036.

(11) (a) Barnett, C. B.; Naidoo, K. J. Free Energies from Adaptive Reaction Coordinate Forces (FEARCF): An Application to Ring Puckering. *Mol. Phys.* **2009**, *107*, 1243−1250. (b) Barnett, C. B.; Naidoo, K. J. Calculating Ring Pucker Free Energy Surfaces from Reaction Coordinate Forces. In *Theory and Applications of Computational Chemistry 2008*; AIP Conference Proceedings; AIP: Shanghai, China, 2009; pp 214−218.

(12) Barnett, C. B.; Naidoo, K. J. Ring Puckering: A Metric for Evaluating the Accuracy of AM1, PM3, PM3CARB-1, and SCC-DFTB Carbohydrate QM/MM Simulations. *J. Phys. Chem. B* **2010**, *114*, 17142−17154.

(13) MacKerel, A. D.; Banavali, N. K. All-atom empirical force field for nucleic acids: 1. Parameter optimization based on small molecule and condensed phase macromolecular target data. *J. Comput. Chem.* **2000**, *21*, 105−120.

(14) Brooks, B. R.; Brooks, C. L., 3rd; Mackerell, A. D., Jr.; Nilsson, L.; Petrella, R. J.; Roux, B.; Won, Y.; Archontis, G.; Bartels, C.;

Boresch, S.; et al. CHARMM: The Biomolecular Simulation Program. *J. Comput. Chem.* **2009**, *30*, 1545−1614.
(15) Elstner, M.; Porezag, D.; Jungnickel, G.; Elsner, J.; Haugk, M.; Frauenheim, T.; Suhai, S.; Seifert, G. Self-Consistent-Charge Density-Functional Tight-Binding Method for Simulations of Complex Materials Properties. *Phys. Rev. B* **1998**, *58*, 7260−7268.
(16) Cui, Q.; Elstner, M.; Kaxiras, E.; Frauenheim, T.; Karplus, M. A QM/MM Implementation of the Self-Consistent Charge Density Functional Tight Binding (SCC-DFTB) Method. *J. Phys. Chem. B* **2000**, *105*, 569−585.
(17) Kumar, S.; Rosenberg, J. M.; Bouzida, D.; Swendsen, R. H.; Kollman, P. A. Multidimensional Free-Energy Calculations Using the Weighted Histogram Analysis Method. *J. Comput. Chem.* **1995**, *16*, 1339−50.
(18) (a) Jorgensen, W. L.; Chandrasekhar, J.; Madura, J. D.; Impey, R. W.; Klein, M. L. Comparison of Simple Potential Functions for Simulating Liquid Water. *J. Chem. Phys.* **1983**, *79*, 926−935. (b) Jorgensen, W. L.; Jenson, C. Temperature Dependence of TIP3P, SPC, and TIP4P Water from NPT Monte Carlo Simulations: Seeking Temperatures of Maximum Density. *J. Comput. Chem.* **1998**, *19*, 1179.
(19) Mao, C.; Cook, W. J.; Zhou, M.; Federov, A. A.; Almo, S. C.; Ealick, S. E. Calf Spleen Purine Nucleoside Phosphorylase Complexed with Substrates and Substrate Analogues. *Biochemistry* **1998**, *37*, 7135−7146.
(20) Humphrey, W.; Dalke, A.; Schulten, K. VMD - Visual Molecular Dynamics. *J. Mol. Graphics* **1996**, *14*, 33−38.
(21) D'Muniz Pereira, H.; Oliva, G.; Garratt, R. C. Purine Nucleoside Phosphorylase from *Schistosoma mansoni* in Complex with Ribose-1-phosphate. *J. Synchrotron Radiat.* **2011**, *18*, 62−65.
(22) Gao, J.; Amara, P.; Alhambra, C.; Field, M. J. A Generalized Hybrid Orbital (GHO) Method for the Treatment of Boundary Atoms in Combined QM/MM Calculations. *J. Phys. Chem. A* **1998**, *102*, 4714−4721.
(23) Frisch, M. J.; Trucks, G. W.; Schlegel, H. B.; Scuseria, G. E.; Robb, M. A.; Cheeseman, J. R.; Montgomery, J. A.; Vreven, T.; Kudin, K. N.; Burant, J. C., et al. *Gaussian 03*, Revision E.01; Gaussian, Inc.: Wallingford, CT, 2003.
(24) (a) Reed, A. E.; Curtiss, L. A.; Weinhold, F. Intermolecular Interactions from a Natural Bond Orbital, Donor−Acceptor Viewpoint. *Chem. Rev.* **1988**, *88*, 899−926. (b) Weinhold, F.; Landis, C. *Valency and Bonding. A Natural Bond Orbital Donor−Acceptor Perspective*; Cambridge University Press: Cambridge, U.K., 2005; p 749.
(25) (a) Bader, R. F. W., *Atoms in Molecules: A Quantum Theory*; Clarendon Press: 1994; (b) Keith, T. A. *AIMAll*, version 13.02.26; TK Gristmill Software: Overland Park, KS, 2012.
(26) Global Minimum, *In this paper, we use the term global minimum to refer to the lowest energy pucker conformer as derived from the semiempirical free energy calculations described above. Note, by definition, each canonical conformer on the pucker FES represents an ensemble of dihedral, bond, and angle conformers that have been conflated to give the optimal pucker free energy for that ring conformer.*
(27) Latha, Y. S.; Yathindra, N. Stereochemical Studies on Nucleic Acid Analogues. I. Conformations of α-Nucleosides and α-Nucleotides: Interconversion of Sugar Puckers via O4′-Exo. *Biopolymers* **1992**, *32*, 249−269.
(28) Barnett, C. B.; Naidoo, K. J. Stereoelectronic and Solvation Effects Determine Hydroxymethyl Conformational Preferences in Monosaccharides. *J. Phys. Chem. B* **2008**, *112*, 15450−15459.
(29) Berti, P. J.; McCann, J. A. Toward a Detailed Understanding of Base Excision Repair Enzymes: Transition State and Mechanistic Analyses of *N*-Glycoside Hydrolysis and *N*-Glycoside Transfer. *Chem. Rev.* **2006**, *106*, 506−555.
(30) Lewandowicz, A.; Schramm, V. L. Transition State Analysis for Human and *Plasmodium falciparum* Purine Nucleoside Phosphorylases. *Biochemistry* **2004**, *43*, 1458−1468.
(31) Appleby, T. C.; Mathews, I. I.; Porcelli, M.; Cacciapuoti, G.; Ealick, S. E. Three-Dimensional Structure of a Hyperthermophilic 5′-Deoxy-5′-methylthioadenosine Phosphorylase from *Sulfolobus solfataricus*. *J. Biol. Chem.* **2001**, *276*, 39232−39242.
(32) Canduri, F.; Silva, R. G.; dos Santos, D. M.; Palma, M. S.; Basso, L. A.; Santos, D. S.; de Azevedo, W. F., Jr. Structure of Human PNP Complexed with Ligands. *Acta Crystallogr. D* **2005**, *61*, 856−862.
(33) Bennett, E. M.; Li, C.; Allan, P. W.; Parker, W. B.; Ealick, S. E. Structural Basis for Substrate Specificity of *Escherichia coli* Purine Nucleoside Phosphorylase. *J. Biol. Chem.* **2003**, *278*, 47110−8.
(34) Canduri, F.; dos Santos, D. M.; Silva, R. G.; Mendes, M. A.; Basso, L. A.; Palma, M. S.; de Azevedo, W. F.; Santos, D. S. Structures of Human Purine Nucleoside Phosphorylase Complexed with Inosine and ddI. *Biochem. Biophys. Res. Commun.* **2004**, *313*, 907−914.
(35) Shi, W.; Ting, L.-M.; Kicska, G. A.; Lewandowicz, A.; Tyler, P. C.; Evans, G. B.; Furneaux, R. H.; Kim, K.; Almo, S. C.; Schramm, V. L. *Plasmodium falciparum* Purine Nucleoside Phosphorylase. *J. Biol. Chem.* **2004**, *279*, 18103−18106.
(36) Barnett, C. B.; Wilkinson, K. A.; Naidoo, K. J. Molecular Details from Computational Reaction Dynamics for the Cellobiohydrolase I Glycosylation Reaction. *J. Am. Chem. Soc.* **2011**, *133*, 19474−19482.